Journal of Solid State Chemistry 184 (2011) 2053–2060

Contents lists available at ScienceDirect

Journal of Solid State Chemistry

journal homepage: www.elsevier.com/locate/jssc

Characterization and photocatalytic activity of Fe- and N-co-deposited TiO_2 and first-principles study for electronic structure

Chung-Chih Yen [a], Da-Yung Wang [b], Li-Shin Chang [a], Han C. Shih [a,c,*]

[a] Department of Materials Science and Engineering, National Chung Hsing University, 250 Kuo Kuang Road, Taichung 40249, Taiwan
[b] Department of Materials Science and Engineering, MingDao University, 369 Wen-Hua Road, Changhua 52345, Taiwan
[c] Institute of Materials Science and Nanotechnology, Chinese Culture University, 55 Hwa-Kang Road, Taipei 11114, Taiwan

ARTICLE INFO

Article history:
Received 29 November 2010
Received in revised form
7 April 2011
Accepted 29 May 2011
Available online 12 June 2011

Keywords:
Titanium dioxide
Photo-catalysis
(Fe,N) co-deposition TiO_2
Band gap energy
First-principle calculation

ABSTRACT

Titanium dioxide (TiO_2), co-deposited with Fe and N, is first implanted with Fe by a metal plasma ion implantation (MPII) process and then annealed in N_2 atmosphere at a temperature regime of 400–600 °C. First-principle calculations show that the (Fe, N) co-deposited TiO_2 films produced additional band gap levels at the bottom of the conduction band (CB) and on the top of the valence band (VB). The (Fe, N) co-deposited TiO_2 films were effective in both prohibiting electron–hole recombination and generating additional Fe–O and N–Ti–O impurity levels for the TiO_2 band gap. The (Fe, N) co-deposited TiO_2 has a narrower band gap of 1.97 eV than Fe-implanted TiO_2 (3.14 eV) and N-doped TiO_2 (2.16 eV). A significant reduction of TiO_2 band gap energy from 3.22 to 1.97 eV was achieved, which resulted in the extension of photocatalytic activity of TiO_2 from UV to Vis regime. The photocatalytic activity and removal rate were approximately two-fold higher than that of the Fe-implanted TiO_2 under visible light irradiation.

1. Introduction

Ever since Fujishima and Honda discovered TiO_2, a number of researchers have been highly interested in this material [1]. However, the wide band gap of TiO_2 (anatase TiO_2 band gap= 3.2 eV) allows activity only under ultraviolet light ($\lambda < 387$ nm), which accounts for only a small part of the solar spectrum (3–5%) [2]. As such, the modification of TiO_2 photocatalytic systems for enhanced activities under visible light ($\lambda > 387$ nm) has become an important research topic in recent years.

The impurity doping of TiO_2 is one strategy used to extend the spectral response of this material to the visible light region. Researchers have used transition metals to enhance the photocatalytic activities of TiO_2. Some metals, such as Fe^{3+}, Cr^{3+}, Co^{2+}, V^{4+}, and Mo^{5+}, enhance the photocatalytic activity of TiO_2 under visible light irradiation [3–7]. However, fast recombination rates prohibit untreated anatase TiO_2 from being used in a wide variety of practical applications. Few metals, such as Fe^{3+} and Cu^{2+}, effectively reduce electron–hole recombination [8,9]. Nonmetal-doped TiO_2 has been proposed to be a promising material with which photo-responses can be extended from the ultraviolet to the visible light region. Some of these nonmetals include B^-, C^-, N^-, S^-, and F^- [10–14]. Anion-doped TiO_2 shows considerable effects on band gap alterations [15]. Among them, N-doped TiO_2 has been proven to be the most effective in narrowing the band gap and in increasing photocatalytic activities in the visible regime [11]. Recent papers have reported the effects of Fe- and N-modification of co-doped TiO_2 in enhancing photocatalysis applications [16–19]. They found that the photocatalytic activities of these powders are about two to four times higher than pure anatase TiO_2 under visible light irradiation. However, the characteristics and electron structures of co-deposited (Fe, N) TiO_2 films by means of experimental and theoretical calculations have yet to be studied.

In this research, we report on the (Fe, N) co-deposited TiO_2 system using a combination of experimental characterizations and theoretical calculations of its electronic structure and density of states (DOS). The local structure around Fe and N in anatase TiO_2 is likewise determined. (Fe, N) co-deposited TiO_2 films were prepared using a metal plasma ion implantation (MPII) technique and then annealed in N_2 atmosphere. MPII [20–22] is a simple method that can modify the physical and chemical performances of films [23,24]. MPII is able to efficiently control the ion distribution, depth, and dosages in the TiO_2 matrix. The as-deposited TiO_2 thin film was subjected to MPII to incorporate the Fe ions, allowing for its steady dispersal onto the surface. However MPII uses a high accelerating voltage to implant metal ions into the TiO_2 matrix, resulting in radiation damage and

* Corresponding author at: Department of Materials Science and Engineering, National Chung Hsing University, 250 Kuo Kuang Road, Taichung 40249, Taiwan. Fax: +886 4 22857017.
E-mail addresses: jackal8914@yahoo.com.tw (C.-C. Yen), hcshih@mx.nthu.edu.tw (H.C. Shih).

0022-4596/$ - see front matter © 2011 Elsevier Inc. All rights reserved.
doi:10.1016/j.jssc.2011.05.036

defects in the implanted samples. The Fe-doped samples were annealed in N_2 atmosphere, both to reduce radiation damage and to incorporate the N ions for the fabrication of visible-light photocatalysts of stable (Fe, N) co-doped TiO_2 films. Here, the co-deposited system demonstrates that Fe and N replace Ti and O in the anatase structure with band gap narrowing. The relationships of the different annealing temperatures on the microstructures, chemical states, optical properties, band structures, and DOS of these (Fe, N) co-deposited TiO_2 films were also investigated. The films manifest higher photocatalytic activities, as evidenced by the photodegradation of methylene blue (MB) solution, under visible light irradiation.

2. Experimental

2.1. Film preparation and characterization

Anatase TiO_2 was prepared by the sol–gel process starting from titanium butoxide precursors. Fe-implanted TiO_2 coatings were fabricated using the MPII technique. After the deposition of the TiO_2 films, Fe ions were implanted into the as-deposited TiO_2 films at an acceleration voltage of 20 keV and an ion dosage of 5×10^{15} ions/cm^2. These conditions are in accordance with our previous experimental results [25]. The Fe-implanted films were annealed in N_2 atmosphere at 400, 500, and 600 °C for 3 h at a heating rate of 5 °C/min. The N_2 flow rate in the furnace was controlled at 100 sccm at 1 atm. The final product of (Fe, N) co-deposited TiO_2 films was thus obtained. For comparison, the as-deposited TiO_2 was annealed in N_2 atmosphere at 500 °C for 3 h.

The crystal structures of the films were measured using grazing incidence X-ray diffraction (GIXRD) (PANalytica X'Per PRO MRD) with the incidence angle of 2° operated at 40 kV and 30 mA with a Cu$K\alpha$ ($\lambda=0.154$ nm) excitation source. The morphology of the (Fe, N) co-deposited TiO_2 coatings was examined by field-emission scanning electron microscopy (FE-SEM; JEOL JSM-6700F) operated at 3 kV. The chemical compositions of the films were determined using X-ray photoelectron spectroscopy (XPS; ULVAC-PHI 5000 VersaProbe; Al$K\alpha$ radiation: 1486.6 eV). The optical absorption of the films was obtained by measuring the absorption edge at 300–800 nm with a UV–visible spectrophotometer (HITACHI U3010).

The photocatalytic activity of (Fe, N) co-deposition TiO_2 coatings was measured by degrading an MB solution. For the photocatalytic experiment, the specimens were placed in a solution containing 20 mL aqueous MB with a concentration of 10^{-6} M under fluorescent light (peaked at $\lambda=452$ and 543 nm) as the irradiation source. The decolorization of the MB solution was measured through a UV–vis spectrometer at 665 nm to monitor the concentration degradation of MB. The removal efficiency of the (Fe, N) co-deposited TiO_2 films was calculated based on the steps detailed below [26]:

$$\text{Removal}\% = \frac{\text{initial concentration} - \text{final concentration}}{\text{initial concentration}} \times 100\%. \quad (1)$$

2.2. Computational methods

The modification of the band gap of the (Fe, N) co-deposited TiO_2 films was investigated using the CASTEP method [27] in Materials Studio 4.0 developed by Accelrys Software Inc. We calculated the band structure of the films using the first-principle density functional theory. Calculations were performed using the spin-polarized density functional theory (DFT) with generalized-gradient-approximation (GGA)/Perdew–Burke–Ernzerhof (PBE) function. We first formed the atomic structure with the optimum lattice constants ($a=0.3776$ nm, $c=0.9486$ nm) of the as-deposited anatase TiO_2, which is consistent with the experimental data. A $7\times3\times3$ Monkhorst–Park grid was used for the irreducible Brillouim zone. The plane-wave kinetic energy cutoff was set as 300 eV. The self-consistent field tolerance was 5.0×10^{-6} eV/atom. The co-deposited system used anatase $1\times2\times1$ supercell, a Ti atom was replaced by a Fe atom, and an O atom was replaced by an N atom [28]. Therefore, the models of energy band gap configuration were compared using four types of $1\times2\times1$ supercells: (a) anatase TiO_2, (b) Fe-implanted TiO_2, (c) N-doped TiO_2, and (d) (Fe, N) co-deposited TiO_2, as shown in Fig. 1.

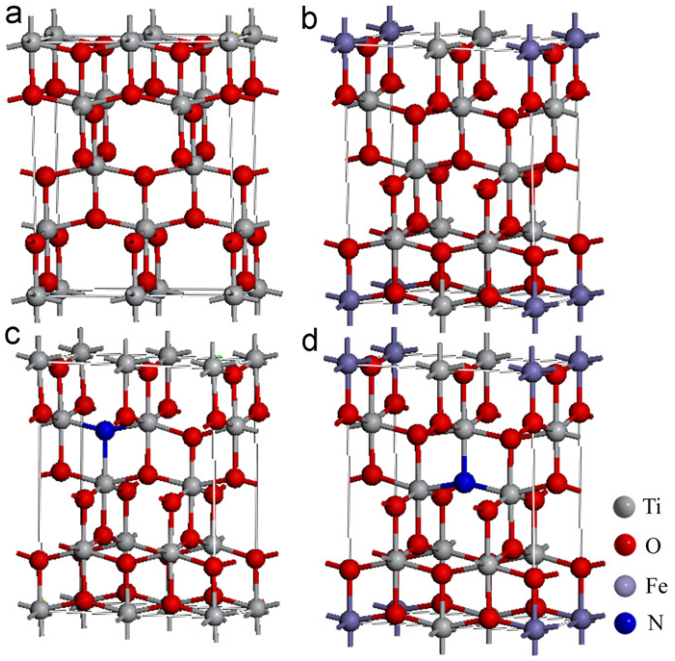

Fig. 1. The $1\times2\times1$ supercell model for (a) anatase TiO_2, (b) Fe-implanted TiO_2, (c) N-doped TiO_2, and (d) (Fe, N) co-deposited TiO_2.

3. Results and discussion

3.1. Microstructure of coatings

Fig. 2 shows the XRD patterns of the (Fe, N) co-deposited TiO_2 films prepared at different temperatures. The results demonstrate the presence of the anatase phase for all co-deposited TiO_2 films at annealing temperatures between 400 and 600 °C. In the previous study [29], we have studied the phase change of TiO_2 calcined at various temperatures. The result indicated that the formation of anatase TiO_2 thin films occurred at calcination temperatures between 400 and 600 °C. The TiO_2 thin films remained amorphous at calcination temperatures below 400 °C. The phase transformation of our MPII-treated TiO_2 from anatase to rutile occurred at 700 °C. It reveals that the phase transformation of the metal-doped TiO_2 from anatase to rutile occurred at temperatures higher than 600 °C. The variation of the phase transformation temperature from that of the pure TiO_2 may be resulted from the impurity effects from the implanted metal ions, which formed strong bonding with the TiO_2 substrate. The crystal size of TiO_2 calcined at various annealing temperatures was calculated based on the Scherrer equation; crystal size of TiO_2 increased to 15, 18, and 20 nm with the increase in the annealing

temperatures. Higher annealing temperatures result in unwanted aggregation. However, at lower annealing temperatures of 400 and 500 °C, crystal size was maintained at less than 20 nm, similar to the as-deposited TiO_2, favoring the maximum lifecycle of excited electrons [30]; therefore, stable co-doped catalyst is obtained. Despite the lower voltage of 20 keV, the intensity of Fe-implanted TiO_2 is slightly decreased by Fe ion implantation compared with as-deposited TiO_2. Thermal annealing was used to improve the structural properties of co-deposited films. The (Fe, N) co-deposited TiO_2 films show the sharpening of diffraction peaks because of the annealing-out of high-energy ion beam-induced defects. The N-doping by thermal annealing is considered beneficial to improve the crystal and without the excessive increase in crystallite size.

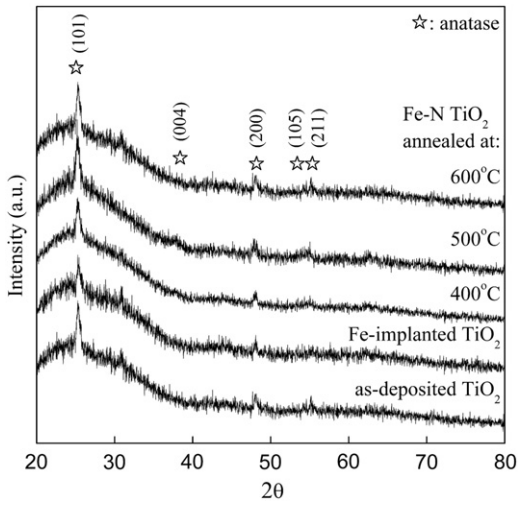

Fig. 2. XRD pattern of the as-deposited TiO_2, Fe-implanted TiO_2, and (Fe, N) co-deposited TiO_2 at the various annealing temperature.

Fig. 3 shows the SEM image of the co-deposited films at various annealing temperatures, with the start of aggregation at above 500 °C. For surface reactions such as photocatalysis, the aggregation surface may be disadvantageous in terms of an increase in effective surface area. The thickness of the (Fe, N) co-deposited TiO_2 films after annealing at various temperatures was measured from cross-sectional morphology, and was revealed to be 100 ± 5 nm, as shown in Fig. 3(d). Therefore, a suitable thermal treatment range not only retains the beneficial morphologies and crystallinity, but also incorporates N into the Fe-implanted TiO_2 thin films.

3.2. Chemical composition

The chemical states of Fe and N incorporated into TiO_2 were measured by XPS. Fig. 4 shows the XPS spectra for the high-resolution N 1*s* and Fe 2*p* core levels of (Fe, N) co-deposited TiO_2 films in N_2 atmosphere at the temperature regime of 400–600 °C. In Fig. 4(a), the relative intensity of the N 1*s* peak increases slightly with increasing annealing temperatures. The concentration of N with N 1*s* in XPS spectra, which may depend on the annealing temperature at 400, 500, and 600 °C, was found to be approximately 0.1, 0.4, and 0.1 at%, respectively. This result implies that the N concentration in the films can be controlled by changing the temperature of the N_2 treatment. However, at 600 °C, the amount of N doped into the TiO_2 lattice reveals a significant decrease because of the higher annealing temperature [31,32]. Typical binding energies of 396–404 eV in N-doped TiO_2 have been observed by several researchers [11,33,34]. The N 1*s* spectra could be deconvoluted into two peaks at 398.2 and 400 eV. The peak at 398.2 eV is attributed to N substitution in O sites and the formation of N–Ti–O bonds in the TiO_2 lattice [32]. In contrast, the slight peak at 400 eV is assigned to the interaction between the N and O characteristics of interstitial N doping, as in N–O bound species [35]. A main peak at the N 1*s* core level located at 398.2 eV corresponds to the substitution of N, which effectively narrows the band gap. This is discussed further later in

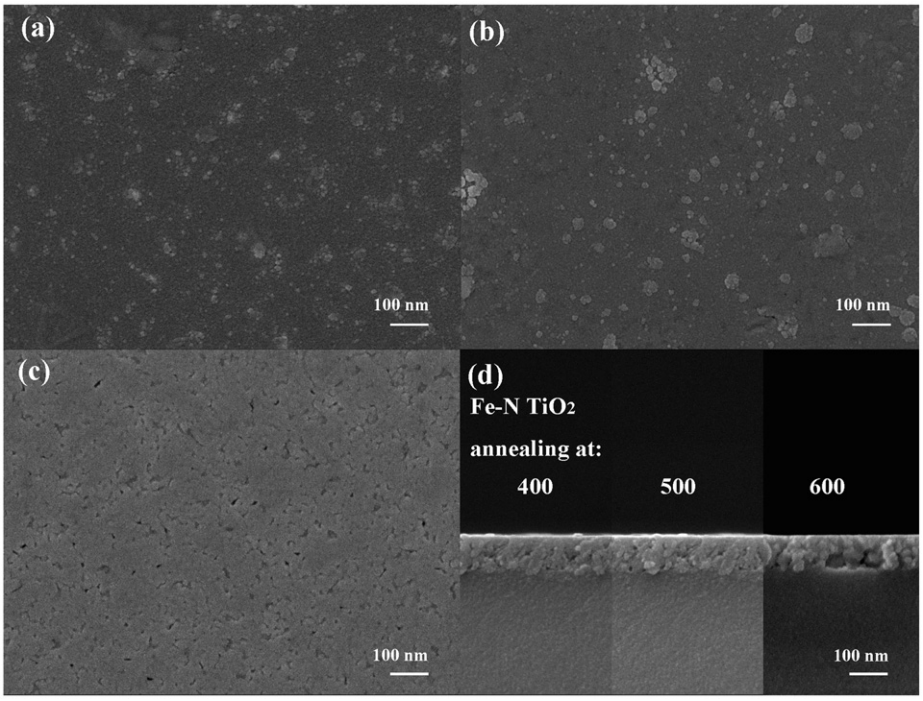

Fig. 3. Surface morphology of the (Fe, N) co-deposited TiO_2 films annealed in N_2 atmosphere at (a) 400 °C, (b) 500 °C, (c) 600 °C, and (d) its cross-sectional morphology.

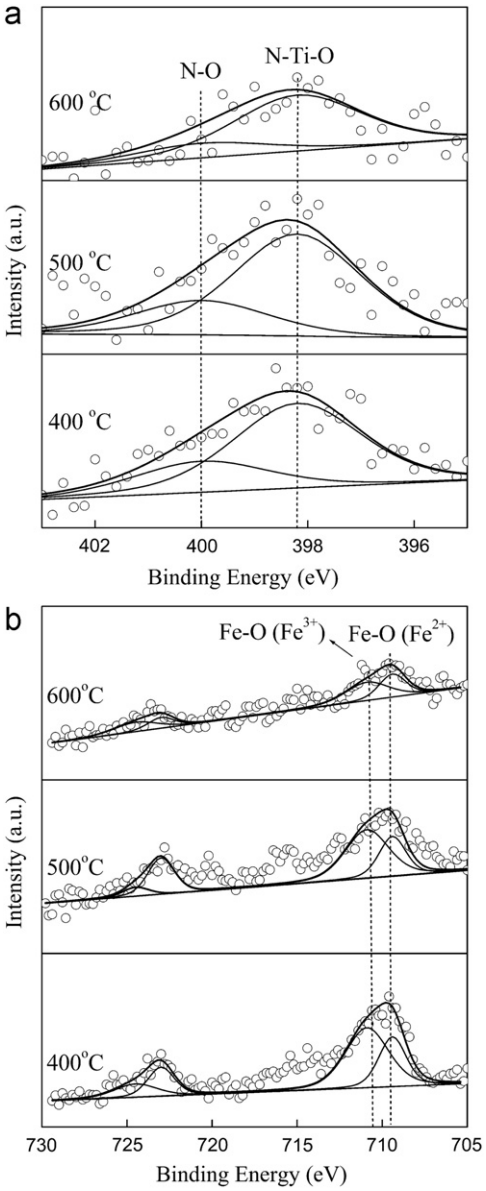

Fig. 4. High resolution (a) N 1*s* and (b) Fe 2*p* XPS spectra of the films prepared at various annealing temperatures in N_2 atmosphere.

this paper. Fig. 4(b) depicts the Fe 2*p* core levels of the films. The Fe 2*p* peaks reveal a weak intensity resulting from the low doping level [36]. Here, Fe^{2+} and Fe^{3+} coexist in the Fe-doped TiO_2 because of the reduction by the electrons generated by the incident light on the TiO_2 materials. The transformation of electron can be shown as $Fe^{3+}+e^{-}\rightarrow Fe^{2+}$. In addition, Fe^{3+} can be easily photo-induced to Fe^{2+} compared with other oxidation potential [37]. However, the main peak in the XPS spectra is at 710.9 eV, and is attributed to Fe^{3+} [38]. Li et al. [39] have reported the preparation of Fe^{3+}-doped TiO_2 by the sol–gel processes. Although these researchers used a precursor to control the chemical states of iron in the TiO_2, the Fe-doped TiO_2 sample also induced a small amount of Fe^{2+}. They considered that the Fe^{2+} favors photocatalytic efficiency; however, the enhancement of photocatalytic activity of Fe-doped TiO_2 composite obviously depended on the Fe^{3+} ion doping. Hence, they frequently redefined the optimal concentration of Fe. The XPS results verify that Fe and N are successfully co-deposited into the TiO_2 lattice.

3.3. Optical analysis and band gap of co-deposited TiO_2 coatings

Fig. 5 shows the optical absorption spectra of films. The co-deposited films demonstrate extended visible-light absorptions higher than those of the as-deposited TiO_2 and N- or Fe-doped TiO_2. The (Fe, N) co-deposited TiO_2 film was annealed under N_2 atmosphere at 500 °C, showing noticeable absorbance at less than 500 nm compared with the Fe or N-doped TiO_2 films and noticeable absorption from 400 to 500 nm. For photocatalysis, the stronger absorption in the visible light can be advantageous in terms of increased effective photosensitivity. The noticeable absorption starts at 500 °C; this can be attributed to N doping in the TiO_2 lattice [11,40]. Asahi et al. [11] calculated the DOS of N-doped TiO_2 and reported that N-doped TiO_2 films noticeably absorbed light at less than 500 nm; this depended on the concentration of N with N 1*s* in the XPS spectra. After being annealed at 500 °C in N_2 atmosphere for 3 h, N was significantly incorporated into the TiO_2 films, as determined by XPS data. The red-shift of the absorption edge of the N-doped TiO_2 films has been attributed to the formation of impurity levels below the TiO_2 conduction band (CB) [18,41]. However, at higher annealing temperatures (e.g., 600 °C), the visible region loss becomes more severe, possibly because of a significant decrease on the amount of N doping on the TiO_2 lattice with an excessive annealing temperature. This hypothesis agrees with XPS analytic results. Thus, the absorption edges of films annealed at higher temperatures did not noticeably absorb light at less than 500 nm.

The optical band gap energies of films can be determined by the Tauc relationship, according to the following formula [42]:

$$(\alpha h\nu)^{1/2} = A(h\nu - Eg), \tag{2}$$

$$\alpha = -1/d\ln(I/Io), \tag{3}$$

where A is the absorption constant, $h\nu$ is the photon energy, α is the absorption coefficient related to transmittance T, d is the film thickness, and I/Io is the transmission intensity. The optical band gap energies of all films were calculated from the Tauc relationship (Fig. 6). The band gap energies are 3.14, 2.16, and 1.97 eV for Fe-doped TiO_2, N-doped TiO_2, and (Fe, N) co-deposited TiO_2, respectively. Among these films, the band gap of (Fe, N) co-deposited TiO_2 is the lowest. In the co-deposited film, two impurity levels are evident in the TiO_2 band. This could be

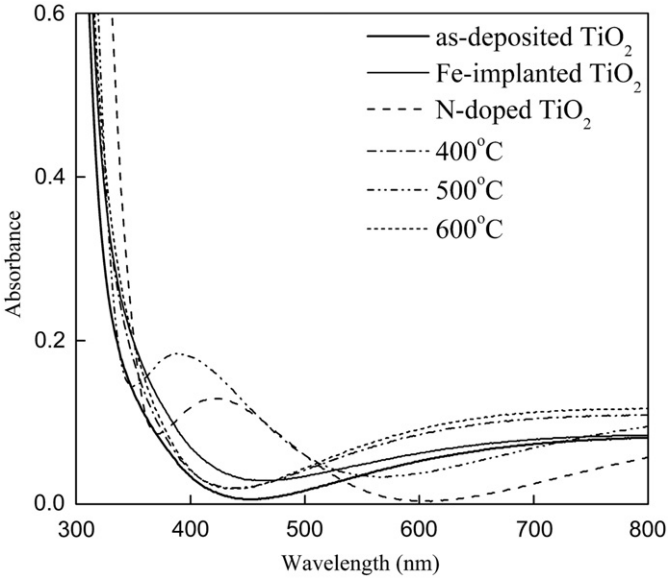

Fig. 5. Optical absorption spectra of (Fe, N) co-deposited TiO_2 films surface treated in N_2 atmosphere in the annealing temperature range of 400–600 °C.

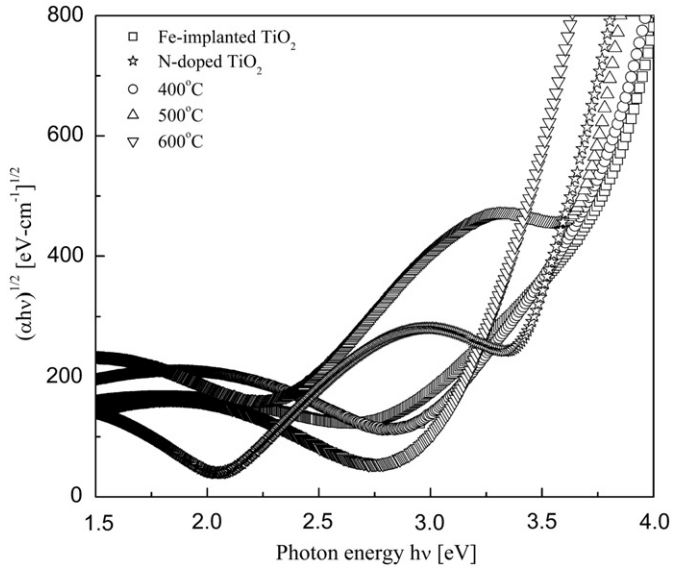

Fig. 6. Tauc plots of $(\alpha h\nu)^{1/2}$ as a function of the photon energy of (Fe, N) co-deposited TiO_2 films with respect to the annealing temperatures.

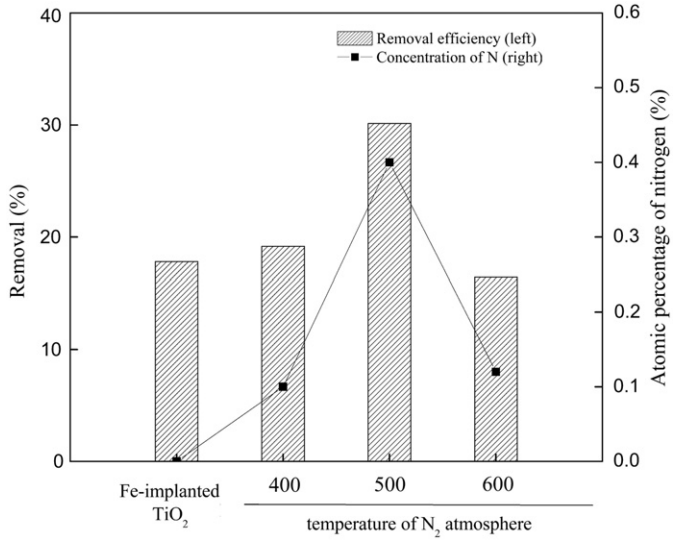

Fig. 7. Removal of MB over (Fe, N) co-deposited TiO_2 films at various annealing temperatures under visible light irradiation.

attributed to the transition processes from the valence band (VB) to the impurity level or from the impurity level to the CB [19]. The co-deposited system seems to favor more visible absorption than that of N or Fe-doped films.

3.4. Photocatalytic activities

The photocatalytic activities of the (Fe, N) co-deposited TiO_2 films were evaluated using the photodegradation of MB solution under visible-light irradiation, as shown in Fig. 7. The best results were obtained from the films annealed at 500 °C, at which temperature the removal rate was 30.1%. In the visible region, the (Fe, N) co-deposited TiO_2 films (annealed at 400 and 500 °C) show higher activities than the Fe-implanted TiO_2 films (17.8%). Nevertheless, at higher annealing temperatures of 600 °C, the photoactivity decreased to 16.4%. The good correspondence between the experimental data and the photoactivity results of (Fe, N) co-deposited TiO_2 films annealed at 600 °C indicates the progressive loss of larger surface areas and of N-doping because of higher treatments. In this experimental range, the optimal annealing temperature is 500 °C. The high photocatalytic activity of the co-deposited film is caused by several factors. First, improved photosensitivity could be attributed to the reduced band gap energy of TiO_2 by the N doping, as demonstrated in the band gap energy calculation results. For the N-doped films, the major role of N doped into TiO_2 is to narrow the band gap, resulting in visible-light photoresponses [35]. Second, when the optimal concentration of Fe^{3+} is doped into the TiO_2, the major role of Fe^{3+} involves increasing carrier centers and improving the trapping efficiency of electrons to inhibit electron–hole recombination [8]. In the previous study [25], it was reported that the optimal value is 0.5 at%. Hence, the co-deposited film could decrease both the band gap and recombination of e^-/h^+pairs to improve the photocatalytic activity in visible-light region.

3.5. Theoretical calculations

The supercell model for the (Fe, N) co-deposited TiO_2 was modeled by a single substitution of Fe and N for the Ti and O atoms, respectively. Fig. 1 shows the supercell model. The band gap energy of the TiO_2 thin film was calculated using the DOS of the substitutional doping of Fe and N in the anatase TiO_2 crystal. Fig. 8 shows the calculated electronic band structures of all films. The evaluated band gap energy is 2.27 eV for as-deposited TiO_2, as shown in Fig. 8(a). The calculated value is lower than the experimental value of 3.22 eV because of the limitation of DFT, because it has a discontinuity of the exchange-correlation energy in DFT [43,44].

The calculated band structures of Fe-doped TiO_2, N-doped TiO_2, and (Fe, N) co-deposited TiO_2 are shown in Figs. 8(b)–(d). For Fe-implanted films, we observed a split in energy levels because of the crystal symmetry and degree of degeneration of coatings after the doping process. An isolated impurity energy level was found below the CB of TiO_2 [Fig. 8(b)]. These impurity energy levels agree well with the CB of TiO_2 and the band gap decreases to 2.18 eV. In the Fe-implanted film, the Fe^{3+} ions were incorporated for the substitution replacement of Ti^{4+} in the TiO_2 lattice and exist in states of Fe^{3+}. They have a half-full *d* orbital, which has a special stability in this kind of electron configuration. Furthermore, Fe^{3+} doping can form a new state for shallow impurity levels in the band gap of TiO_2.

For the N-doped TiO_2, an upward shift toward the top of the VB led to the narrowing of the band gap energy to 1.89 eV, as shown in Fig. 8(c). The band gap is narrower compared to that of Fe-implanted TiO_2. For N substitution in TiO_2 lattice, the combination of the N 2*p* and O 2*p* states is the most effective way to narrow the band gap. These states introduced by N are shallow in the gap above the valence band.

For the (Fe, N) co-deposited TiO_2 [Fig. 8(d)] film, a downward shift toward the bottom of the CB and an upward shift toward the top of the VB cause narrowing of the band gap energy to 0.9 eV lower than that of mono-doped TiO_2. These results demonstrate that the co-deposited film could form the two impurity levels within the band gap of TiO_2. Furthermore, the reduction regime of the band gap between VB and CB is more significant than that in the Fe or N-doped TiO_2. For the calculations, the addition of a scissor operation of 0.95 eV to the calculated band gap is dependent on the difference between the calculated band gap (3.22 eV) and the experimental type (2.27 eV). As a benchmark for comparison, the band gap used the results from Fe-implanted TiO_2, N-doped TiO_2, and (Fe, N) co-deposited TiO_2 calculations, and the band gaps are 3.13, 2.84, and 1.85 eV, respectively. This rationalizes the experimental data, showing that the fundamental absorption edges of (Fe, N) co-deposited TiO_2 red-shifted toward the visible-light regime (Fig. 5) and exhibited lower band gap

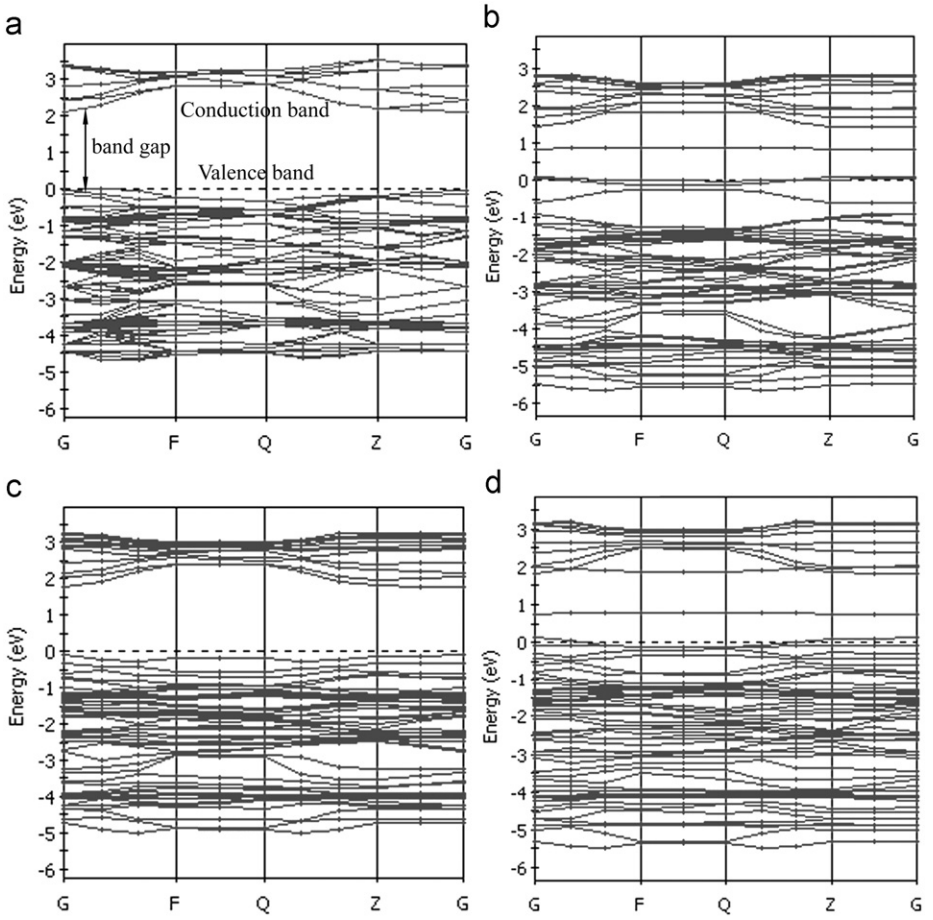

Fig. 8. Calculated electronic band structures for (a) anatase TiO_2, (b) Fe-implanted TiO_2, (c) N-doped TiO_2, and (d) (Fe, N) co-deposited TiO_2 thin films.

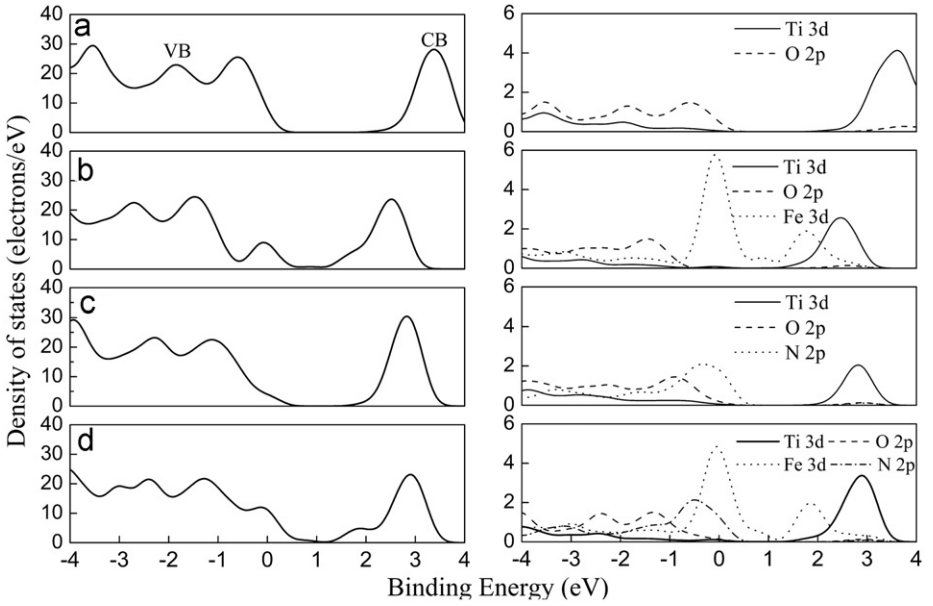

Fig. 9. Total density of states (left) and partial density of states (right) for (a) anatase TiO_2, (b) Fe-implanted TiO_2, (c) N-doped TiO_2, and (d) (Fe, N) co-deposited TiO_2 thin films.

energies (Fig. 6) compared with Fe or N-doped TiO_2. Thus, Fe and N co-deposition can further modify the band structure and improve the sensitivity of the film to visible light.

To further understand the changes in the band gap of co-deposited TiO_2, the calculated DOS is illustrated in Fig. 9, including the total density of states (TDOS) and partial density of states (PDOS) of as-deposited TiO_2, Fe-implanted TiO_2, N-doped TiO_2, and (Fe, N) co-deposited TiO_2. The Fermi energy (E_F) is located at the 0 eV binding energy. The CB and VB of the TiO_2 correspond to the Ti 3*d* and O 2*p* states, respectively.

The incorporation of Fe and N atoms results in different *d* and *p* orbitals in connection with the Ti 3*d* and O 2*p* states. The co-deposited TiO_2 system is able to modify both CB and VB after the doping process.

For the Fe-implanted TiO_2 [Fig. 9(b)], the shallow donor levels near the CB after the Ti atom is replaced by an Fe atom, and the impurity of the Fe 3*d* states appear below the Ti 3*d* states, which is attributed to Fe e_g orbital contribution. As a result, the band gap of the Fe-implanted TiO_2 is slightly reduced. This kind of impurity state is located above E_F, which can improve electron trapping in shallow trapping sites, thereby separating the arrival times between the electron–hole pairs at the surface [45]. These gap states are able to act as electron traps and enhance photocatalytic activities. The experimental work on the Fe-implanted TiO_2 reveals a significant increase in photocatalytic activity compared with the as-deposited TiO_2. A significant peak near the Fermi level could be observed, which is mainly attributed to the Fe t_{2g} orbital contribution. These impurity states are located at the Fermi level, which implies easy electron transition to CB. However, these impurity states result in deep trapping. When the concentration of Fe^{3+} ions is higher, the impurities become the recombination centers that increase the e^-/h^+recombination, leading to poor photocatalytic activities [46].

For the N-doped TiO_2, Fig. 9(c) shows the shallow acceptor for the N 2*p* states located near the O 2*p* states. This impurity level shows the advantage of better photo-excited carrier migration over deeper impurity levels because deep impurity levels are able to act as recombination centers and reduce photo-excited carrier migration [11,47,48]. In contrast, hybridization between the N 2*p* and O 2*p* states occurred near the Fermi level to form continuum states results in strong mixing at the O 2*p* states. This shows that the continuum states form after the N-doping. For photocatalysis, the continuum states can be advantageous in terms of increased effective photo-excited carrier migration compared with Fe-doped TiO_2. Similar results were reported by Long and English [49] and Mi et al. [50], indicating that the hybrid continuum states are unable to function as a recombination center because of the presence of fully occupied states.

As for the (Fe, N) co-deposited TiO_2 [Fig. 9(d)], shallow donor and shallow acceptor were induced close to the CB and VB levels in the narrowing band, which corresponds to the experimental work. The (Fe, N) co-deposited TiO_2 structure showed narrowed band gaps with higher photocatalytic efficiency under visible-light radiation, similar to some reports in literature [19]. Nevertheless, our results differ from the findings of Liu et al. [17], which showed lower photocatalytic activity of (Fe, N) co-doped TiO_2 compared with those in single doping; this may be attributable to the dopant concentration. Some investigations on co-doping systems have considered the relation between photocatalytic activity and dopant concentration [18,19]. When the dopant concentration is higher than the optimal value, the dopant transforms into recombination centers, resulting in an increase in e^-/h^+ recombination, and, consequently, poor photocatalytic activity. In the present study, MPII could efficiently control ion distribution and ion dosages in the TiO_2 matrix. Thus, we expect that a small amount of Fe ions would disperse on the surface layer of the TiO_2, leading to an enhanced photocatalytic activity.

4. Conclusions

(Fe, N) co-deposited TiO_2 films were successfully synthesized using the MPII technique in conjunction with a heat treatment process. The N doping can effectively decrease the band gap. The formation of N–Ti–O bonds was observed in the impurity level of TiO_2 coatings after N_2 treatment and an effective band gap modification. In addition, N-doping in Fe-implanted TiO_2 films extended the absorption edge, which was red-shifted toward the visible light region. The band gap energy of the (Fe, N) co-deposited TiO_2 films was reduced by 0.23–1.25 eV after annealing in N_2 atmosphere. The reduction of the band gap energy resulted in the increased photosensitivity of TiO_2 in the visible light regime. The films annealed in N_2 atmosphere at 500 °C demonstrated the best photocatalytic activity and degradation efficiency, reaching values that are about two-fold higher than those of Fe-implanted TiO_2 under visible light irradiation. Moreover, the energetic and electronic properties of (Fe, N) co-deposited TiO_2 films were evaluated by the theoretical first-principle calculations. (Fe, N) co-deposited TiO_2 films were found to be highly effective potocatalysts. This design also responded to the visible light regime. The shallow acceptor and donor also formed in the band gap of TiO_2. It is strongly suggested that (Fe, N) co-deposited TiO_2 films not only enable easy photo-excited electron–hole separation, but also reduce the band gap significantly. These results suggest that the proposed (Fe, N) co-deposited TiO_2 film design conforms to the requirements for highly effective photocatalysts under visible light irradiation.

References

[1] A. Fujishima, K. Honda, Nature 238 (1972) 37–38.
[2] T. Sasaki, Supramol. Sci. 5 (1998) 367–371.
[3] W. Choi, A. Termin, M.R. Hoffman, J. Phys. Chem. 98 (1994) 13669–13679.
[4] K. Nagaveni, M.S. Hegde, G. Madras, J. Phys. Chem. B 108 (2004) 20204–20212.
[5] J. Zhu, Z. Deng, F. Chen, J. Zhang, H. Chen, M. Anpo, J. Huang, L. Zhang, Appl. Catal. B 62 (2006) 329–335.
[6] A.D. Paola, G. Marci, L. Palmisano, M. Schiavello, K. Uosaki, S. Ikeda, B. Ohtani, J. Phys. Chem. B 106 (2002) 637–645.
[7] J. Yin, X. Zhao, J. Phys. Chem. B 110 (2006) 12916–12925.
[8] E.C. Butler, A.P. Davis, J. Photochem. Photobiol. A 70 (1993) 273–283.
[9] M. Fujihira, Y. Satoh, T. Osa, Bull. Chem. Soc. Jpn. 55 (1982) 666–671.
[10] X. Chen, Y. Lou, C. Anna, S. Samia, C. Burda, J.L. Gole, Adv. Funct. Mater. 15 (2005) 41–49.
[11] R. Asahi, T. Morikawa, T. Ohwaki, K. Aoki, Y. Taga, Science 293 (2001) 269–271.
[12] T. Umebayashi, T. Yamaki, H. Itoh, K. Asai, Appl. Phys. Lett. 82 (2002) 454–456.
[13] G. Wu, A. Chen, J. Photochem. Photobiol. A 195 (2008) 47–53.
[14] C.D. Valentin, G. Pacchioni, A. Selloni, Phys. Rev. B 70 (2004) 085116.
[15] T. Umebayashi, T. Yamaki, S. Yamamoto, A. Miyashita, S. Tanaka, T. Sumita, K. Asai, J. Appl. Phys. 93 (2003) 5156–5160.
[16] K.S. Rane, R. Mhalsiker, S. Yin, T. Sato, Kuk Cho, E. Dunbar, P. Biswas, J. Solid State Chem. 179 (2006) 3033–3044.
[17] Z. Liu, Y. Wang, W. Chu, Z. Li, C. Ge, J. Alloys Compd. 501 (2010) 54–59.
[18] H. Hao, J. Zhang, Microporous Mesoporous Mater. 121 (2009) 52–57.
[19] Y. Cong, J. Zhang, F. Chen, M. Anpo, D. He, J. Phys. Chem. C 111 (2007) 10618–10623.
[20] Z. Yi, Z. Xiao, F. Ma, T. Zhang, Y. Li, Surf. Coat. Technol. 128–129 (2000) 186–191.
[21] G.B. Stachowiak, G.W. Stachowiak, P. Evans, Wear 241 (2000) 220–227.
[22] C.L. Chang, D.Y. Wang, Nucl. Instrum. Methods B 194 (2002) 463–468.
[23] H. Yamashita, M. Harada, J. Misaka, M. Takeuchi, Y. Ichihashi, F. Goto, M. Ishida, T. Sasaki, M. Anpo, J. Synchrotron Radiat. 8 (2001) 569–571.
[24] R. Fromkmecht, I. Khubeis, S. Massing, O. Meyer, Nucl. Instrum. Methods Phys. Res. Sec. B 147 (1999) 191–201.
[25] C.C. Yen, D.Y. Wang, M.H. Shih, L.S. Chang, H.C. Shih, Appl. Surf. Sci. 256 (2010) 6865–6870.
[26] J. Yu, H. Yu, C.H. Ao, S.C. Lee, J.C. Yu, W. Ho, Thin Solid Films 496 (2006) 273–280.
[27] M.D. Segall, P.J.D. Lindan, M.J. Probert, C.J. Pickard, P.J. Hasnip, S.J. Clark, M.C. Payne, J. Phys.: Condens. Matter 14 (2002) 2717–2744.
[28] Z. Zhao, Q. Liu, Catal. Lett. 124 (2008) 111–117.
[29] D.Y. Wang, H.C. Lin, C.C. Yen, Thin Solid Films 515 (2006) 1047–1052.
[30] Z. Zhang, C.C. Wang, R. Zakaria, J.Y. Ying, J. Phys. Chem. B 102 (1998) 10871–10878.
[31] T. Ohno, T. Mitsui, M. Matsumura, Chem. Lett. 32 (2003) 364–365.
[32] X. Chen, C. Burda, J. Phys. Chem. B 108 (2004) 15446–15449.
[33] S. Sakthivel, M. Janczarek, H. Kisch, J. Phys. Chem. B 108 (2004) 19384–19387.
[34] M. Sathish, B. Viswanathan, R.P. Viswanath, C.S. Gopinath, Chem. Mater. 17 (2005) 6349–6353.

[35] J.A. Rodriguez, T. Jirsak, J. Dvorak, S. Sambasivan, D. Fischer, J. Phys. Chem. B 104 (2000) 319–328.
[36] J. Zhua, F. Chena, J. Zhang, H. Chenb, M. Anpob, J. Photochem. Photobiol. A 180 (2006) 196–204.
[37] J. Ma, Y. Wei, W.X. Liu, W.B. Cao, Res. Chem. Intermed. 35 (2009) 329–336.
[38] H.B. Jinag, L. Gao, Mater. Chem. Phys. 77 (2002) 878–881.
[39] Y.J. Li, J. Li, M.Y. Ma, Y.Z. Ouyang, W.B. Yan, Sci. China Ser. B Chem. 52 (2009) 1113–1119.
[40] T. Sano, N. Negishi, K. Koike, K. Takeuchi, S. Matsuzawa, J. Mater. Chem. 14 (2004) 380–384.
[41] S. Sato, S. Nakanura, S. Abe, Appl. Catal. A 284 (2005) 131–137.
[42] J. Tauc, Phys. Status Solidi 15 (1966) 627–637.
[43] C.D. Valentin, G. Pacchioni, A. Selloni, S. Livraghi, E. Giamello, J. Phys. Chem. B 109 (2005) 11414–11419.
[44] J.P. Perdew, M. Levy, Phys. Rev. Lett. 51 (1983) 1884–1887.
[45] Z. Zhang, C.C. Wang, R. Zakaria, J.Y. Ying, J. Phys. Chem. B 102 (1998) 10871–10878.
[46] C.Y. Wang, D.W. Bahnemann, J.K. Dohrmann, Chem. Commun. 16 (2000) 1539–1540.
[47] J. Tang, Z. Zou, J. Ye, Catal. Lett. 92 (2004) 53–56.
[48] J. Sato, H. Kobayashi, Y. Inoue, J. Phys. Chem. B 107 (2003) 7970–7975.
[49] R. Long, N.J. English, Appl. Phys. Lett. 94 (2009) 132102.
[50] L. Mi, P. Xu, H. Shen, P.N. Wang, Appl. Phys. Lett. 90 (2007) 171909.